Vacuum 132 (2016) 70–81

Contents lists available at ScienceDirect

Vacuum

journal homepage: www.elsevier.com/locate/vacuum

Numerical analysis of fluid transport phenomena and spiking defect formation during vacuum electron beam welding of 2219 aluminium alloy plate

Chengcai Liu*, Jingshan He

State Key Laboratory of Advanced Welding and Joining, Harbin Institute of Technology, Harbin 150001, China

ARTICLE INFO

Article history:
Received 12 May 2016
Received in revised form
25 July 2016
Accepted 25 July 2016
Available online 27 July 2016

Keywords:
Vacuum electron beam welding
Mathematical model
Heat transfer
Fluid flow
Keyhole backfilling
Spiking defect

ABSTRACT

In this paper, a 3D mathematical model is proposed to investigate the physical transport phenomena in weld pool and vapour plume during the stationary vacuum electron beam welding on 2219 aluminium alloy plate. Three beam current cases are employed to investigate the heat transfer, fluid flow, keyholing, keyhole backfilling and collapsing processes, and the resulting spiking defect and residual crater. In the model, a keyhole-tracing heat source is adopted to simulate the energy interactions between electron beam and material with the help of VOF technique. Results indicate that the beam profile and heat flux distribution decreases the growing speed of keyhole dimensions. The increase of beam current raises the evaporation intensity, keyhole wall temperature, keyholing depth and keyhole instability. On the premise of same heating time, a larger beam current produces a spiking defect in partially-penetrated weld. Finally, all the simulation results are validated against experiments.

1. Introduction

2219 aluminium alloy, as a kind of age hardening Al–Cu alloy, is widely applied in aerospace industry, due to its high specific strength and excellent heat resistance [1]. In view of its high thermal conductivity, to obtain sound welds, electron beam welding (EBW) operated in vacuum is the most favourite [2]. It is a deep-penetration welding method that utilizes the focused electron beam in vacuum as a high-power density heat source to melt and evaporate the workpiece and produce a weld seam with a large depth-to-width ratio and narrow heat-affected zone [3]. Keyhole, as a typical characteristic of deep-penetration welding methods, has been found to be unstable and fluctuating [4–6], which plays a significant role in the weld formation and quality [7–10]. For example, keyhole's collapse phenomena often induce the formation of void-type defects such as pore, porosity, or cold shut, etc [11–16]. So it is necessary to investigate the keyhole's dynamic behaviour involving heat transfer, keyhole evolution and fluid flow and induced void-type defects.

So far, quite a few experimental researches based on X-ray camera, CCD camera, secondary emitted beams and photodiodes technologies have been done to detect in real-time the EBW's keyhole formation and fluctuation [4,5]. However, in view of the expensive observation equipments and observation difficulties in vacuum, numerical simulations are more desirable for researchers to discover and understand the complex physical phenomena. However, at present, most of numerical investigations in EBW field have mainly concentrated on the thermal effect and related stress issues [3,17,18]. Relevant researches on the fluid flow and keyhole's dynamic mechanism are very limited. In order to enhance the understanding of EBW's transport phenomena, Rai et al. [19] analyzed the keyhole wall temperature variation in depth and fluid flow behaviour at different input powers during EBW of 21Cr–6Ni–9Mn steel and Ti–6Al–4V alloy and compared with that of laser welding samples. Results indicate that the keyhole wall temperature in vacuum EBW is below the boiling point at 1 atm as the laser welding did due to the ambient pressure. In addition, it is found that the lower keyhole wall temperature in EBW induces a stronger Marangoni convection compared to that in laser welding. Besides, Rai et al. [20] further studied the transport phenomena during EBW of 304 L stainless steel and discovered similar regularities. Their works lay a foundation for the present numerical simulation of EBW's transport phenomena. However, the evolution

* Corresponding author. Tel./fax: +86 451 86412911.
E-mail address: liuchengcai1983@163.com (C. Liu).

http://dx.doi.org/10.1016/j.vacuum.2016.07.033
0042-207X/

of keyhole shape was not considered in their works, which has been known to a critical factor affecting the weld quality. Besides, another objective of this work is to explore the formation mechanism of spiking defect, which is one of void-type defects. Schauer et al. [15] in 1978 predicted the spiking tendency in EBW seam from the perspective of the keyhole instability caused by the competing effects of recoil pressure and surface tension by measuring the keyhole wall temperature distribution. However, their prediction results are mainly based on the dimensionless temperature analysis on the postulated keyhole shape due to the former computation limitations. Similarly, Wei et al. [16] theoretically predicted the formations of spiking and humping through scale analysis. In addition, Luo et al. [21] indirectly predicted the cavity defect formation by a two-dimensional fractional flow model describing bubble flow in EBW pool. However, the influence of keyhole was neglected in their research.

In this paper, a 3D mathematical model is proposed to study the physical transport phenomena during the stationary EBW process on 20 mm thick 2219 aluminium alloy plate. Three study cases with different beam currents are employed to analyze the interaction between electron beam and material, melting, evaporation, fluid flow, the formation and collapse of keyhole as well as the spiking defect formation. Finally, the experiments are implemented to validate the model.

2. Mathematical modelling

The following assumptions are introduced in this paper: (1) the initial temperature of the workpiece is 293 K. The vacuum chamber is filled with 10^{-2} Pa low-pressure gas. (2) Weld pool and metal vapour are assumed to be incompressible Newtonian laminar flow. (3) Plasma formation and multiple reflections are neglected when high voltage electron beam is adopted [19]. (4) The boiling point of the alloy is dependent on the local pressure in the keyhole.

2.1. Governing equations

Based on the above assumptions, the governing equations of mass, momentum, energy and volume fraction in Cartesian coordinates are expressed as follow:

Mass conservation equation

$$\nabla\cdot \mathrm{U} = 0 \tag{1}$$

Momentum conservation equation

$$\rho\left(\frac{\partial \mathrm{U}}{\partial t} + \nabla\cdot(\mathrm{UU})\right) = \nabla\cdot(\mu\nabla \mathrm{U}) - \nabla p + \frac{(1-f_\mathrm{l})^2}{\left(f_\mathrm{l}^3 + B\right)} A_\mathrm{mush}\mathrm{U} + \rho g \tag{2}$$

Energy conservation equation

$$\frac{\partial}{\partial t}(\rho h) + \nabla\cdot(\rho \mathrm{U} h) = \nabla\cdot(k\nabla T) \tag{3}$$

VOF equation

$$\frac{\partial F}{\partial t} + \mathrm{U}\cdot\nabla F = 0 \tag{4}$$

where **U** represents the velocity vector. ρ, μ, p, k represent the density, dynamic viscosity, pressure, thermal conductivity. The third term of right-hand side of Eq. (2) represents the momentum sink governing the velocity of solid phase, liquid phase and mushy zone introduced by enthalpy-porosity technique. f_l, A_mush, B represent the liquid fraction, mushy zone constant and a small positive number (0.001) to prevent division by zero. t, h, T and **g** denote time, material enthalpy, temperature and gravitational acceleration. Eq. (4) is employed by multiphase model VOF to trace the transient keyhole profile, in which F represents the volume fraction function. The material enthalpy h is also handled by the enthalpy-porosity technique to help account for the solid-liquid phase transition [22]:

$$h = h_\mathrm{ref} + \int_{T_\mathrm{ref}}^{T} C_\mathrm{p}dT + f_\mathrm{l}H_\mathrm{f} \tag{5}$$

$$f_\mathrm{l} = \begin{cases} 0 & T < T_\mathrm{s} \\ \dfrac{T-T_\mathrm{s}}{T_\mathrm{l}-T_\mathrm{s}} & T_\mathrm{s} \le T \le T_\mathrm{l} \\ 1 & T > T_\mathrm{l} \end{cases} \tag{6}$$

where h_ref and T_ref are the reference enthalpy and reference temperature, H_f is the latent heat of fusion, T_s and T_l are the solidus temperature and liquidus temperature.

2.2. Boundary conditions

The computational domain consisting of gas phase (mixture of low pressure gas and metal vapour) and solid substrate for the stationary EBW process is demonstrated in Fig. 1. O_1O_2 is the symmetry axis. AB, AC and BD are the pressure outlets of gas phase domain. CE, DF and EF are wall boundaries of solid substrate. Detailed boundary conditions are described as follow:

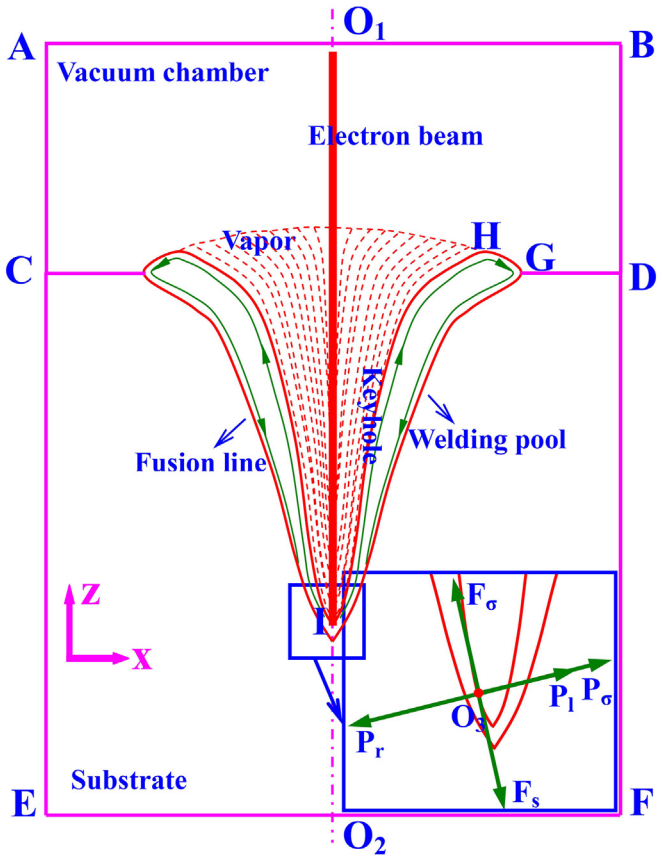

Fig. 1. Computational domain and boundaries during the stationary EBW process.